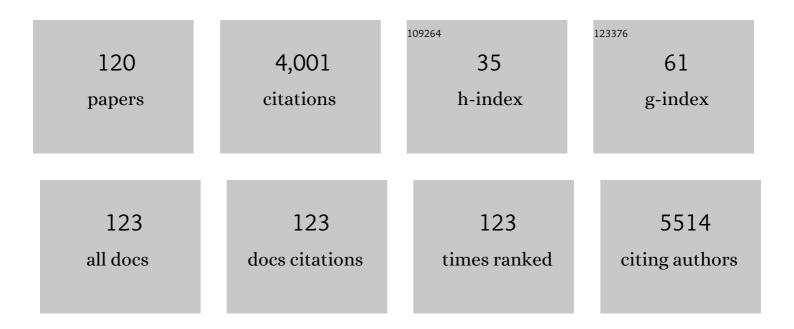
List of Publications by Year in descending order

Source: https://exaly.com/author-pdf/383310/publications.pdf Version: 2024-02-01



#	Article	IF	CITATIONS
1	Effect of annealing on grain growth and Y segregation behavior in tetragonal ZrO <sub>2</sub> thin film. Journal of the American Ceramic Society, 2022, 105, 2300-2308.	1.9	1
2	Factors limiting quantitative phase retrieval in atomic-resolution differential phase contrast scanning transmission electron microscopy using a segmented detector. Ultramicroscopy, 2022, 233, 113457.	0.8	5
3	Fluoride-ion conversion alloy for fluoride-ion batteries. Journal of Materials Chemistry A, 2022, 10, 3743-3749.	5.2	4
4	Atomic-Level Changes during Electrochemical Cycling of Oriented LiMn <sub>2</sub> O <sub>4</sub> Cathodic Thin Films. ACS Applied Materials & Interfaces, 2022, 14, 6507-6517.	4.0	9
5	Direct Observation of Atomistic Reaction Process between Pt Nanoparticles and TiO <sub>2</sub> (110). Nano Letters, 2022, 22, 4161-4167.	4.5	9
6	Atomic-resolution STEM image denoising by total variation regularization. Microscopy (Oxford,) Tj ETQq0 0 0 rgE	BT /Oyerloo	ck 10 Tf 50 5
7	Probing the meta-stability of oxide core/shell nanoparticle systems at atomic resolution. Chemical Engineering Journal, 2021, 405, 126820.	6.6	8
8	Room temperature fluoride ion conductivity in defective β-KSb1-δF4-3δ polycrystals. Journal of Power Sources, 2021, 483, 229173.	4.0	4
9	Direct imaging of atomistic grain boundary migration. Nature Materials, 2021, 20, 951-955.	13.3	94
10	Anataselike Grain Boundary Structure in Rutile Titanium Dioxide. Nano Letters, 2021, 21, 2745-2751.	4.5	9
11	Automated geometric aberration correction for large-angle illumination STEM. Ultramicroscopy, 2021, 222, 113215.	0.8	4
12	Direct visualization of anionic electrons in an electride reveals inhomogeneities. Science Advances, 2021, 7, .	4.7	24
13	Atomic-Resolution Topographic Imaging of Crystal Surfaces. ACS Nano, 2021, 15, 9186-9193.	7.3	7
14	Two-Dimensional Room-Temperature Giant Antiferrodistortive SrTiO3 at a Grain Boundary. Physical Review Letters, 2021, 126, 225702.	2.9	7
15	Atomistic Origin of Li-Ion Conductivity Reduction at (Li <sub>3<i>x</i></sub> La <sub>2/3–<i>x</i></sub> )TiO <sub>3</sub> Grain Boundary. Nano Letters, 2021, 21, 6282-6288.	4.5	20
16	Development of High-Speed Scan System for Atomic Resolution STEM. Microscopy and Microanalysis, 2021, 27, 2710-2712.	0.2	0
17	Direct atomistic defect observations by depth sectioning and dynamic STEM. Microscopy and Microanalysis, 2021, 27, 2138-2139.	0.2	0
18	Flexoelectric nanodomains in rare-earth iron garnet thin films under strain gradient. Communications Materials, 2021, 2, .	2.9	10

#	Article	IF	CITATIONS
19	Improving the depth resolution of STEM-ADF sectioning by 3D deconvolution. Microscopy (Oxford,) Tj ETQq1 1	0.784314	rg&T /Overlo
20	Reprint of: Automated geometric aberration correction for large-angle illumination STEM. Ultramicroscopy, 2021, 231, 113410.	0.8	0
21	Single-source-precursor synthesis and high-temperature evolution of novel mesoporous SiVN(O)-based ceramic nanocomposites. Journal of the European Ceramic Society, 2020, 40, 6280-6287.	2.8	11
22	TV-rate Atomic-resolution STEM Imaging. Microscopy and Microanalysis, 2020, 26, 1150-1151.	0.2	0
23	Ultrafast Encapsulation of Metal Nanoclusters into MFI Zeolite in the Course of Its Crystallization: Catalytic Application for Propane Dehydrogenation. Angewandte Chemie, 2020, 132, 19837-19842.	1.6	3
24	Stabilization of a honeycomb lattice of IrO6 octahedra by formation of ilmenite-type superlattices in MnTiO3. Communications Materials, 2020, 1, .	2.9	5
25	Metastable oxysulfide surface formation on LiNi <sub>0.5</sub> Mn <sub>1.5</sub> O <sub>4</sub> single crystal particles by carbothermal reaction with sulfur-doped heterocarbon nanoparticles: new insight into their structural and electrochemical characteristics, and their potential applications, lournal of Materials Chemistry A, 2020, 8, 22302-22314.	5.2	17
26	Atomic structures of Tiâ€doped αâ€Al 2 O 3 Σ13 grain boundary with a small amount of Si impurity. Journal of the American Ceramic Society, 2020, 103, 6659-6665.	1.9	6
27	Dislocation and oxygen-release driven delithiation in Li2MnO3. Nature Communications, 2020, 11, 4452.	5.8	41
28	PPARα Ligand-Binding Domain Structures with Endogenous Fatty Acids and Fibrates. IScience, 2020, 23, 101727.	1.9	41
29	Phase-Contrast-Based Structure Retrieval Methods in Atomic Resolution Scanning Transmission Electron Microscopy – When They Hold and When They Don't. Microscopy and Microanalysis, 2020, 26, 442-443.	0.2	1
30	Synthesis of Novel Melilite-Type Iron/Cobalt Oxides and Their Oxygen Evolution Reaction Electrocatalytic Activity. Chemistry of Materials, 2020, 32, 6847-6854.	3.2	5
31	Phase relation between supercooled liquid and amorphous silicon. Applied Physics Letters, 2020, 116, 093705.	1.5	2
32	Three-Dimensional Imaging of a Single Dopant in a Crystal. Physical Review Applied, 2020, 13, .	1.5	27
33	Direct Measurement of Electronic Band Structures at Oxide Grain Boundaries. Nano Letters, 2020, 20, 2530-2536.	4.5	38
34	Ultrafast Encapsulation of Metal Nanoclusters into MFI Zeolite in the Course of Its Crystallization: Catalytic Application for Propane Dehydrogenation. Angewandte Chemie - International Edition, 2020, 59, 19669-19674.	7.2	63
35	Reversible Electrochemical Insertion/Extraction of Magnesium Ion into/from Robust NASICON-Type Crystal Lattice in a Mg(BF <sub>4</sub> ) <sub>2</sub> -Based Electrolyte. ACS Applied Energy Materials, 2020, 3, 6824-6833.	2.5	14
36	Grain boundary Li-ion conductivity in (Li0.33La0.56)TiO3 polycrystal. Applied Physics Letters, 2020, 116, .	1.5	24

RYO ISHIKAWA

#	Article	IF	CITATIONS
37	Discovery of Ternary Silicon Titanium Nitride with Spinel-Type Structure. Scientific Reports, 2020, 10, 7372.	1.6	8
38	High spatiotemporal-resolution imaging in the scanning transmission electron microscope. Microscopy (Oxford, England), 2020, 69, 240-247. First-principles calculations of group IA and group IV impurities in simplimath	0.7	27
39	xmlns:mml="http://www.w3.org/1998/Math/MathML"> <mml:mrow><mml:mi>α</mml:mi><mml:mtext>â^'<!--<br-->mathvariant="normal"&gt;A<mml:msub><mml:mi mathvariant="normal"&gt;I<mml:mn>2</mml:mn></mml:mi </mml:msub><mml:msub><mml:mi mathvariant="normal"&gt;O<mml:mn>3</mml:mn></mml:mi </mml:msub></mml:mtext></mml:mrow> .	mml:mtext> 0.9	<mml:mi 11</mml:mi 
40	Physical Review Materials, 2020, 4. Improving the Depth Resolution of HAADF Sectioning by 3D Deconvolution. Microscopy and Microanalysis, 2020, 26, 3110-3111.	0.2	2
41	Transition-Metal Distribution in Brownmillerite Ca <sub>2</sub> FeCoO <sub>5</sub> . Inorganic Chemistry, 2019, 58, 10209-10216.	1.9	3
42	Fast Li-ion conduction at grain boundaries in (La,Li)NbO3 polycrystals. Journal of Power Sources, 2019, 441, 227187.	4.0	24
43	Atomic Scale Origin of Enhanced Ionic Conductivity at Crystal Defects. Nano Letters, 2019, 19, 2162-2168.	4.5	30
44	Coexistence of two different atomic structures in the Σ13 pyramidal twin boundary in α-Al <sub>2</sub> O <sub>3</sub> . Philosophical Magazine Letters, 2019, 99, 435-443.	0.5	4
45	Large angle illumination enabling accurate structure reconstruction from thick samples in scanning transmission electron microscopy. Ultramicroscopy, 2019, 197, 112-121.	0.8	12
46	Electric Field Imaging at Atomic Resolution by DPC STEM. Materia Japan, 2019, 58, 104-104.	0.1	0
47	Direct Electric Field Imaging of Atomistic Graphene Defects. Nihon Kessho Gakkaishi, 2019, 61, 231-236.	0.0	0
48	Atomic-scale structure relaxation, chemistry and charge distribution of dislocation cores in SrTiO3. Ultramicroscopy, 2018, 184, 217-224.	0.8	45
49	Picometer-scale atom position analysis in annular bright-field STEM imaging. Ultramicroscopy, 2018, 184, 177-187.	0.8	47
50	Unique fitting of electrochemical impedance spectra by random walk Metropolis Hastings algorithm. Journal of Power Sources, 2018, 403, 184-191.	4.0	18
51	Direct electric field imaging of graphene defects. Nature Communications, 2018, 9, 3878.	5.8	74
52	Resolution Achievement of 40.5 pm in Scanning Transmission Electron Microscopy using 300 kV Microscope with Delta Corrector. Microscopy and Microanalysis, 2018, 24, 120-121.	0.2	6
53	Overall water splitting by Ta3N5 nanorod single crystals grown on the edges of KTaO3 particles. Nature Catalysis, 2018, 1, 756-763.	16.1	390
54	Atomic-Scale Measurement of Flexoelectric Polarization at <mml:math xmlns:mml="http://www.w3.org/1998/Math/MathML" display="inline"&gt;<mml:mrow><mml:msub><mml:mrow><mml:mi>SrTiO</mml:mi></mml:mrow><mml:mn>3 Dislocations. Physical Review Letters, 2018, 120, 267601.</mml:mn></mml:msub></mml:mrow></mml:math 	<	/mml:msub>

#	Article	IF	CITATIONS
55	Probing the Internal Atomic Charge Density Distributions in Real Space. ACS Nano, 2018, 12, 8875-8881.	7.3	43
56	Influence of Dislocations in Transition Metal Oxides on Selected Physical and Chemical Properties. Crystals, 2018, 8, 241.	1.0	54
57	Surface and Electric Field Imaging by Newly Designed Atomic-Resolution STEM. Microscopy and Microanalysis, 2018, 24, 118-119.	0.2	0
58	Attainment of 40.5 pm spatial resolution using 300 kV scanning transmission electron microscope equipped with fifth-order aberration corrector. Microscopy (Oxford, England), 2018, 67, 46-50.	0.7	51
59	Electron microscope control and image analysis by DigitalMicrograph. Materia Japan, 2018, 57, 584-588.	0.1	0
60	Atomic-Scale Tracking of a Phase Transition from Spinel to Rocksalt in Lithium Manganese Oxide. Chemistry of Materials, 2017, 29, 1006-1013.	3.2	32
61	Relative Li-ion mobility mapping in Li <sub>0.33</sub> La <sub>0.56</sub> TiO <sub>3</sub> polycrystalline by electron backscatter diffraction and electrochemical strain microscopy. Applied Physics Express, 2017, 10, 061102.	1.1	13
62	Possible absence of critical thickness and size effect in ultrathin perovskite ferroelectric films. Nature Communications, 2017, 8, 15549.	5.8	104
63	One-pot synthesis of a C/SiFeN(O)-based ceramic paper with in-situ generated hierarchical micro/nano-morphology. Journal of the European Ceramic Society, 2017, 37, 5193-5203.	2.8	16
64	Single-source-precursor derived RGO/CNTs-SiCN ceramic nanocomposite with ultra-high electromagnetic shielding effectiveness. Acta Materialia, 2017, 130, 83-93.	3.8	86
65	Transparent polycrystalline cubic silicon nitride. Scientific Reports, 2017, 7, 44755.	1.6	57
66	Single-atom dynamics in scanning transmission electron microscopy. MRS Bulletin, 2017, 42, 644-652.	1.7	33
67	Full picture discovery for mixed-fluorine anion effects on high-voltage spinel lithium nickel manganese oxide cathodes. NPG Asia Materials, 2017, 9, e398-e398.	3.8	22
68	Room-temperature dilute ferromagnetic dislocations in Sr1â^'xMnxTiO3â^'δ. Physical Review B, 2017, 96, .	1.1	6
69	Quantitative electric field mapping in thin specimens using a segmented detector: Revisiting the transfer function for differential phase contrast. Ultramicroscopy, 2017, 182, 258-263.	0.8	36
70	Better Contrast for Imaging Defects by ABF. Microscopy and Microanalysis, 2017, 23, 480-481.	0.2	0
71	Three-Dimensional Point Defect Imaging by Large-angle Illumination STEM. Microscopy and Microanalysis, 2017, 23, 424-425.	0.2	1
72	Single-source-precursor synthesis and electromagnetic properties of novel RGO–SiCN ceramic nanocomposites. Journal of Materials Chemistry C, 2017, 5, 7950-7960.	2.7	48

#	Article	IF	CITATIONS
73	A new method to detect and correct sample tilt in scanning transmission electron microscopy bright-field imaging. Ultramicroscopy, 2017, 173, 76-83.	0.8	21
74	Quantitative Relation Between Differential Phase Contrast Images Obtained by Segmented and Pixelated Detectors. Microscopy and Microanalysis, 2017, 23, 440-441.	0.2	0
75	Electric field imaging of single atoms. Nature Communications, 2017, 8, 15631.	5.8	144
76	Direct Electromagnetic Structure Observation by Aberration-corrected Differential Phase Contrast Scanning Transmission Electron Microscopy. Microscopy and Microanalysis, 2016, 22, 906-907.	0.2	1
77	Atomic Structure and Properties of Dislocations and Grain Boundaries. , 2016, , .		0
78	Quantitative Atomic Resolution Differential Phase Contrast Imaging Using a Segmented Area All Field Detector. Microscopy and Microanalysis, 2016, 22, 504-505.	0.2	1
79	Single atom visibility in STEM optical depth sectioning. Applied Physics Letters, 2016, 109, .	1.5	40
80	Interfacial Atomic Structure of Twisted Few-Layer Graphene. Scientific Reports, 2016, 6, 21273.	1.6	18
81	Atomic-Resolution Composition Mapping in EDS STEM. Microscopy and Microanalysis, 2016, 22, 1432-1433.	0.2	2
82	Jointed magnetic skyrmion lattices at a small-angle grain boundary directly visualized by advanced electron microscopy. Scientific Reports, 2016, 6, 35880.	1.6	27
83	Adsorption sites of single noble metal atoms on the rutile TiO <sub>2</sub> (1 1 0) surface influenced by different surface oxygen vacancies. Journal of Physics Condensed Matter, 2016, 28, 175002.	0.7	7
84	Direct visualization of lithium via annular bright field scanning transmission electron microscopy: a review. Microscopy (Oxford, England), 2016, 66, 3-14.	0.7	20
85	Atomic mechanism of polarization-controlled surface reconstruction in ferroelectric thin films. Nature Communications, 2016, 7, 11318.	5.8	61
86	An artificial photosynthesis anode electrode composed of a nanoparticulate photocatalyst film in a visible light responsive GaN-ZnO solid solution system. Scientific Reports, 2016, 6, 35593.	1.6	19
87	Materials Characterization with Quantitative Electron Microscopy. Materia Japan, 2016, 55, 479-483.	0.1	1
88	Misalignment Induced Artifacts in Quantitative Annular Bright-Field Imaging. Microscopy and Microanalysis, 2016, 22, 888-889.	0.2	7
89	Complex Point Defect Structure in Cubic Boron Nitride. Materia Japan, 2016, 55, 609-609.	0.1	0
90	Atomic Observation of Phase Transformation from Spinel to Rock Salt in Lithium Manganese Oxide. Microscopy and Microanalysis, 2015, 21, 333-334.	0.2	0

#	Article	IF	CITATIONS
91	Quantitative Electron Microscopy and the Application by Single Electron Signals. Microscopy and Microanalysis, 2015, 21, 1449-1450.	0.2	0
92	Advanced Electron Microscopy for Energy Related Materials. Microscopy and Microanalysis, 2015, 21, 471-472.	0.2	0
93	Annular Bright-Field Electron Microscopy Tracking Solid-State Chemical Reaction. Microscopy and Microanalysis, 2015, 21, 963-964.	0.2	0
94	B11-O-11Atomic-scale Tracking Cation Diffusion in Lithium Manganese Oxide. Microscopy (Oxford,) Tj ETQq0 0 (	0 rgBT /Ov 9.7	rerlock 10 Tf S
95	Atomic-scale assessment of the crystallization onset in silicon carbonitride. Journal of the European Ceramic Society, 2015, 35, 3355-3362.	2.8	15
96	Towards 3D Mapping of BO <sub>6</sub> Octahedron Rotations at Perovskite Heterointerfaces, Unit Cell by Unit Cell. ACS Nano, 2015, 9, 8412-8419.	7.3	78
97	Visualizing the Mixed Bonding Properties of Liquid Boron with High-Resolution X-Ray Compton Scattering. Physical Review Letters, 2015, 114, 177401.	2.9	13
98	Large-angle illumination STEM: Toward three-dimensional atom-by-atom imaging. Ultramicroscopy, 2015, 151, 122-129.	0.8	54
99	Direct Imaging of Pt Single Atoms Adsorbed on TiO <sub>2</sub> (110) Surfaces. Nano Letters, 2014, 14, 134-138.	4.5	115
100	Atomic-scale origin of the large grain-boundary resistance in perovskite Li-ion-conducting solid electrolytes. Energy and Environmental Science, 2014, 7, 1638.	15.6	219
101	Quantitative Annular Dark Field Electron Microscopy Using Single Electron Signals. Microscopy and Microanalysis, 2014, 20, 99-110.	0.2	80
102	Direct Observation of Dopant Atom Diffusion in a Bulk Semiconductor Crystal Enhanced by a Large Size Mismatch. Physical Review Letters, 2014, 113, 155501.	2.9	91
103	Enhancing Photocatalytic Activity of LaTiO <sub>2</sub> N by Removal of Surface Reconstruction Layer. Nano Letters, 2014, 14, 1038-1041.	4.5	129
104	Three-Dimensional Location of a Single Dopant with Atomic Precision by Aberration-Corrected Scanning Transmission Electron Microscopy. Nano Letters, 2014, 14, 1903-1908.	4.5	89
105	Tracking Dopant Diffusion Pathways inside Bulk Materials. Microscopy and Microanalysis, 2014, 20, 50-51.	0.2	0
106	Atomic-Resolution Monitoring of Structural Phase Transition in Bi-magnetic Core/Shell Oxide Nanoparticles. Microscopy and Microanalysis, 2014, 20, 106-107.	0.2	0
107	Toward 3D Mapping of Octahedral Rotations at Perovskite Thin Film Heterointerfaces Unit Cell by Unit Cell. Microscopy and Microanalysis, 2014, 20, 1038-1039.	0.2	0
108	Atomic Structure of Luminescent Centers in High-Efficiency Ce-doped w-AlN Single Crystal. Scientific Reports, 2014, 4, 3778.	1.6	43

#	Article	IF	CITATIONS
109	Direct Atomicâ€Resolution Observation of Two Phases in the Li <sub>1.2</sub> Mn <sub>0.567</sub> Ni <sub>0.166</sub> Co <sub>0.067</sub> O <sub>2</sub> Cathode Material for Lithiumâ€Ion Batteries. Angewandte Chemie - International Edition, 2013, 52, 5969-5973.	7.2	242
110	Multivariate Statistical Characterization of Charged and Uncharged Domain Walls in Multiferroic Hexagonal YMnO <sub>3</sub> Single Crystal Visualized by a Spherical Aberration-Corrected STEM. Nano Letters, 2013, 13, 4594-4601.	4.5	46
111	Cubic Cesium Hydrogen Silicododecatungstate with Anisotropic Morphology and Polyoxometalate Vacancies Exhibiting Selective Water Sorption and Cation-Exchange Properties. Chemistry of Materials, 2013, 25, 905-911.	3.2	42
112	Functional Complex Point-Defect Structure in a Huge-Size-Mismatch System. Physical Review Letters, 2013, 110, 065504.	2.9	40
113	Persistence of Covalent Bonding in Liquid Silicon Probed by Inelastic X-Ray Scattering. Physical Review Letters, 2012, 108, 067402.	2.9	63
114	Direct Imaging of Hydrogen Atoms in a Crystal by Annular Bright-field STEM. Microscopy and Microanalysis, 2011, 17, 1278-1279.	0.2	0
115	Direct Imaging of Interstitial Atoms in a Complex (La0.6Er0.4)5Ni19 Hydrogen-Storage Compound. Microscopy and Microanalysis, 2011, 17, 1612-1613.	0.2	0
116	Direct imaging of hydrogen-atom columns in a crystal by annular bright-field electron microscopy. Nature Materials, 2011, 10, 278-281.	13.3	313
117	Stacking Faults and a Novel Structural Polytype in a Hydrogen-Storage (La <sub>0.8</sub> Mg <sub>0.2</sub> )Ni <sub>3.5</sub> Alloy with Block-Stacking Superstructures. Materials Transactions, 2009, 50, 943-947.	0.4	0
118	Novel-long period structures in hydrogen storage LaxY1â^²xNi3.8compounds. Acta Crystallographica Section A: Foundations and Advances, 2008, 64, C533-C533.	0.3	0
119	Thermophysical properties of the melts of AlPdMn icosahedral quasicrystal. Philosophical Magazine, 2007, 87, 2965-2971.	0.7	8
120	A Compton scattering study on the Hume-Rothery mechanism of AlCu–TM (TM: transition metal) quasicrystals. Journal of Physics Condensed Matter, 2006, 18, 7203-7208.	0.7	0